Scripta Materialia 122 (2016) 102–105

Contents lists available at ScienceDirect

Scripta Materialia

journal homepage: www.elsevier.com/locate/scriptamat

Regular Article

Impurity-driven formation of branched pores in porous anodic alumina

Byeol Kim [a,1], Yong Youn [b,1], Yi-Seul Park [a], Dal Nim Moon [a], Kyungtae Kang [c], Seungwu Han [b], Jin Seok Lee [a,*]

[a] Department of Chemistry, Sookmyung Women's University, Seoul 140-742, South Korea
[b] Department of Materials Science and Engineering and Research Institute of Advanced Materials, Seoul National University, Seoul 151-755, South Korea
[c] Department of Applied Chemistry, Kyung Hee University, Yongin, Gyeonggi 446-701, South Korea

ARTICLE INFO

Article history:
Received 21 April 2016
Accepted 17 May 2016
Available online 2 June 2016

Keywords:
Anodic aluminum oxide
Impurity
Branched pore
Electric-field distribution
Current-density distribution

ABSTRACT

Understanding of pore formation in porous anodic alumina is prerequisite for realizing its potential applications in the field of nanofabrication. Here, we explored the impurity-driven pore formation of porous anodic alumina via a two-step anodization process in acid solution with various applied voltages. We varied the purity of Al foil, and found that the branching and bending of pores displayed by low-purity Al foils are originated from an electric-field imbalance that results from the presence of impurities. Also, the pore formation mechanism and characteristic geometry induced by the impurities within the Al foil were investigated using experimental and simulation models.

Owing to the unique self-ordering properties in nanometer scale, porous anodic aluminum oxide (AAO), typically formed by the electrochemical oxidation of Al in acidic solutions, has been extensively investigated for application in the field of nanofabrication [1–3]. It is generally believed that the anodization current during the steady-state growth of the porous film is mainly related to the movement of ionic species (Al^{3+}, O^{2-}, and OH^-) through the oxide layer at the bottom of the pores for the pore formation. While Al^{3+} ions are directly injected into the electrolyte, the oxide film is formed at the metal/oxide interface, due to the migration of OH^-/O^{2-} species. As a result of the incorporation of the electrolyte species, an anion-contaminated layer is formed [4–7]. This field-assisted dissolution model suggests that the development of a porous film results from the equilibrium established between the formation of the oxide at the metal/oxide interface and the field-enhanced dissolution at the oxide/electrolyte interface [8,9]. The evolution and development of porous films arise from the viscous flow of alumina from the bottom of the pores toward the cell walls, which is driven by film growth [4,5].

A porous anodic alumina film with hexagonally close-packed pores is typically obtained through a self-organized two-step anodization process [10]. The stress placed on the anodic film during pore formation is evenly distributed over the entire film area [11,12]; consequently, the resulting porous film exhibits a self-ordered, hexagonal close packing of the pores. And, the characteristic parameters of porous anodic alumina, such as pore diameter (D_p), inter-pore distance, and oxide-film thickness can be controlled by adjusting the anodizing conditions, including the type of electrolyte, temperature, applied potential, current density, and duration of the first anodization process [13–18]. Additionally, the anodization response is highly dependent on the purity of the Al foil employed; impurities contained within the Al foil can change the flow of ions during the electrochemical reactions that lead to pore formation [19–24]. Recent studies have investigated the migration of anion species into the oxide film formed on the surface of the Al substrate during anodization that leads to a considerable accumulation of impurities in the barrier layer [21]. The local accumulation of alloying elements in a given region of the metal/oxide interface can change the local rates of pore formation [19,20]. Moreover, it has been reported that impurities at the metal/oxide interface—the primary location of oxide growth—may inhibit the formation of the aluminum oxide [21,22]. Consequently, changes in the oxidation reactions due to impurities can ultimately result in the formation of non-uniform oxidation cracks and flaws on the film surface [24].

In this work, we present a comparative study of the characteristic geometry of porous anodic alumina films prepared from three Al foils of different purity (99.999%, 99.5%, and 99.0%) via a two-step anodization process in oxalic acid solution at various applied voltages. To explore the effect of impurities in low-purity Al foil on the electrochemical reaction rates, oxidation, and dissolution, we investigated the structural features of the anodic alumina films using experiments and simulation models to confirm the growth mechanism induced by the impurities within the Al foil.

To fabricate a porous alumina membrane, three types of Al foils of different purity (99.999% ($Al_{99.999}$), 99.5% ($Al_{99.5}$), and 99.0% ($Al_{99.0}$)) were anodized via a two-step process in 0.3 M oxalic acid solution at an applied voltage of 40 V and a temperature of 10 °C (see the experimental details in supplementary information). The scanning electron

* Corresponding author.
E-mail address: jinslee@sookmyung.ac.kr (J.S. Lee).
[1] These authors contributed equally.

http://dx.doi.org/10.1016/j.scriptamat.2016.05.026
1359-6462/

microscopy (SEM) images in Fig. 1a–c show that the anodized alumina film obtained from $Al_{99.999}$ has a hexagonally ordered pore array with most of the pores being circular in shape, but, when the Al purity is reduced, the array regularity and the circularity of the pores are degraded. In particular, anodized alumina film using $Al_{99.0}$ exhibits a disordered pore array featuring distinctly non-circular pore shapes; these appear to overlap with adjacent pores, resulting in a sub-pore structure alongside the main pore array.

Previous studies have shown that the presence of impurities can influence the local rates of oxidation and consequently affect the oxide morphology [19,20]. Interestingly, even a tiny amount of impurities in the Al foil can exert a strong effect on the alumina film morphology, including defects, D_p, and film thickness. Here, we define defects as the irregular pores, which are not circular. As the purity of the Al foil decreased, the defect percentage increased (Fig. S1a) and the D_p values decreased (Fig. S1b). The alumina film resulting from the anodization of $Al_{99.0}$ showed a high defect percentage of ~60%, a slightly smaller pore diameter of ~41 nm, and a relatively large standard deviation as a consequence of a greater number of elliptical pores. Generally, for anodization with a conventional potentiostatic system, the D_p values of an anodic alumina film increase linearly with the applied potential, at a rate of ~0.9 nm V^{-1} [25]. However, the present study indicates that the D_p values can be also affected by the purity of the employed Al foil. The final morphology of the alumina films depends on the impurities, which introduce disordered pore arrays and non-uniform pore shapes, resulting in an irregular D_p. The occluded impurities in the Al foil induce an unbalanced local chemical reaction rate [19,20], which triggers disordered pore formation and causes the formation of defects in the alumina film; this in turn reduces its growth rate. The side-view SEM images of the alumina films with different impurity (insets of Fig. 1a–c) confirm the changes in film thickness, which shows the alumina film thickness after anodization as a function of the purity of the Al foil. In particular, the thickness of the anodized film decreased from 2.07 μm for $Al_{99.999}$ to 1.78 μm for $Al_{99.0}$ (Fig. S1c). Therefore, it supports that the presence of impurities at the metal/oxide interface can effectively retard the growth of the oxide. Impurities in the Al foils may not be evenly distributed, and can aggregate to form "islands of impurities".

In order to confirm this hypothesis, low-magnification SEM images of the anodized alumina samples were analyzed. In particular, the top-view image of the anodized alumina film obtained with $Al_{99.0}$ reveals a large number of defects as well as a putative lump of impurity (Figs. 1d and S2). Energy-dispersive X-ray spectroscopy (EDX) mapping data shows that the main impurity components of this "island of impurities" are Si and Fe, which are concentrated in the tubular island; this suggests that the occluded impurities can block the electrochemical reactions related to the pore formation. These findings indicate that impurities are locally distributed and can trigger a change in the anodic alumina formation [24].

In the side-view image of the alumina film displayed in Fig. 1f, a very large void (white arrow), which corresponds to a defect, can be observed. We can thus assume that the impurities are degraded on the anodic alumina film and have a significant effect on local pore morphologies, thereby inducing transformations in the pore structure. Moreover, if located inside the bulk Al, the impurities can affect the formation of a straight pore channel. Fig. 1e–f shows the directions along which pores were formed on porous alumina films prepared with Al foils of different purity. Anodized films derived from the low-purity $Al_{99.0}$ foils exhibited tilted arrays of pore channels progressed along a specific direction to avoid the impurity [26], while the high-purity $Al_{99.999}$ foil showed an upright pore channel perpendicular to the bulk Al; this behavior may be due to the local position of the impurities. In this study, these impurity driven branching and transformation of pore arrays have often been observed at the pore bottom even after anodizing for 10 h.

Based on our initial results and preliminary hypotheses, we then investigated the effect of the electric field as the main driving force on the pore growth during anodization as well as the effect of the impurities on the direction of the electric field. The branched pore-growth mechanism in the impurity-laden film was investigated with an ion-current simulation model [4,24,27]. Anodization during the steady-state growth of the porous alumina involves a cross transport of ionic species for pore formation. Fig. 2a–c shows the simulated electric-field distribution and ionic-current density, based on the geometric parameter of produced pore channel (Fig. S3). It is seen that a small lump of impurities (circle)

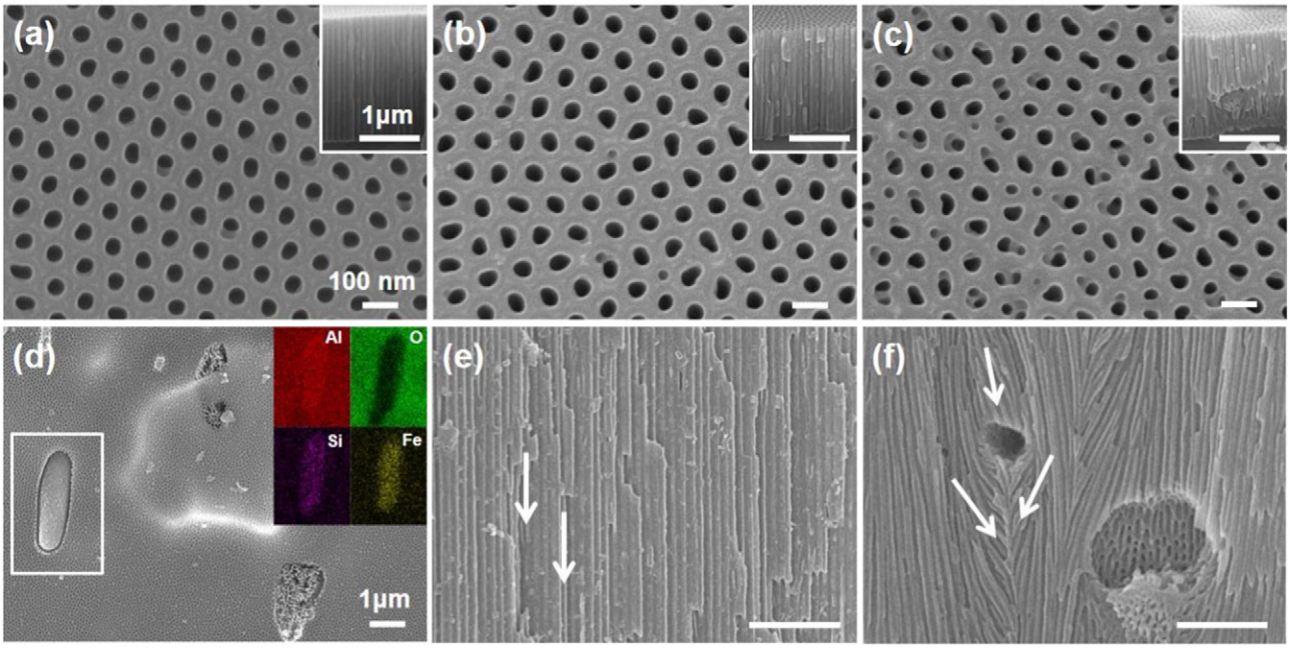

Fig. 1. SEM images of porous anodic alumina anodized using Al foils of different purity: (a) 99.999%, (b) 99.5%, and (c) 99.0%. Insets show side-view SEM images of the corresponding alumina films. (d) Top-view SEM image of the porous alumina anodized using 99.0% Al foils. Inset shows EDX analysis of the impurity composition in the area outlined by the white square. (e, f) Side-view SEM images of porous anodic alumina anodized using (e) 99.999% and (f) 99.0% Al foil, respectively. White arrows indicate the direction of pore arrays.

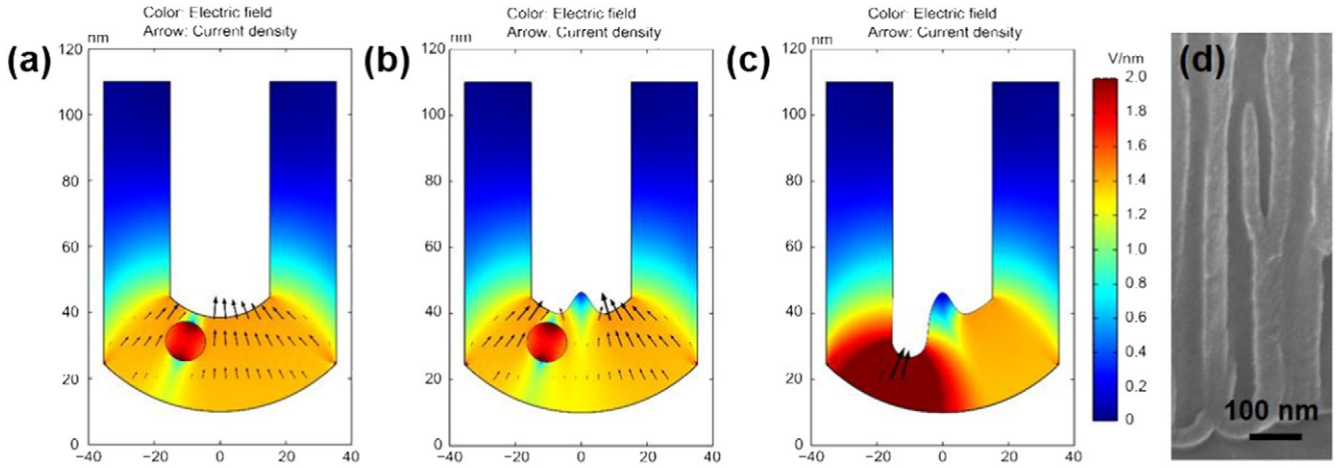

Fig. 2. (a)–(c): Time-dependent electric field (color) and current-density (black arrows) distribution in the aluminum oxide with the Si impurity (red circle). (d) Side-view SEM image of a branched pore induced by impurities during anodization.

in the Al film significantly affects the nearby electric field and ion currents because the impurity blocks the ionic movement, and the ions must therefore detour around the impurity. Interestingly, the oxide formation rate, which is related to the current density, changes locally near the impurity. That is to say, the rate is reduced immediately in front of the impurity, while it is enhanced at the pore center. The Al oxide formation (i.e., the volume expansion) is enhanced in the region with a higher electric field, while the oxide dissolution is predominant in the region in front of the impurity, because the ion flow is blocked by the impurity. Thus, the simulation results in Fig. 2a suggest an intermediate geometry as shown in Fig. 2b. As the oxide solvates in front of the impurity, the thickness of the oxide film is reduced. Indeed, the SEM image in Fig. 1f shows that when the large impurity is exposed to the electrolyte, it quickly dissolves due to the electric field. This leads to the formation of branched-pore geometries (Fig. 2c). The final shape is consistent with the SEM images of the porous alumina in Fig. 2d. The present simulation confirms that the branched pores are formed alongside the main pore channel because of the imbalanced electric field induced by the impurity.

The local variation of the electric field induced by impurities can affect the pore formation during anodization. Furthermore, the electric field can be adjusted according to the applied potential [28,29]. To explore the local variation of the electric field depended on applied voltage during anodization, different voltages were applied to the Al foils of different purity. The size of the hexagonal cells and thus D_p increased when the applied voltage was increased (Fig. S4). For instance, the D_p values at an applied voltage of 50 V were larger than those at 30 V (Fig. 3a). As observed in the porous alumina obtained at an applied voltage of 40 V (Fig. S1), impurities have a strong influence on pore geometries and diameter. For instance, D_p in the anodized $Al_{99.0}$ was relatively small (~30 nm at 30 V, and ~50 nm at 50 V), with a large standard deviation due to the high degree of defect percentage (~61% at 30 V, and ~52% at

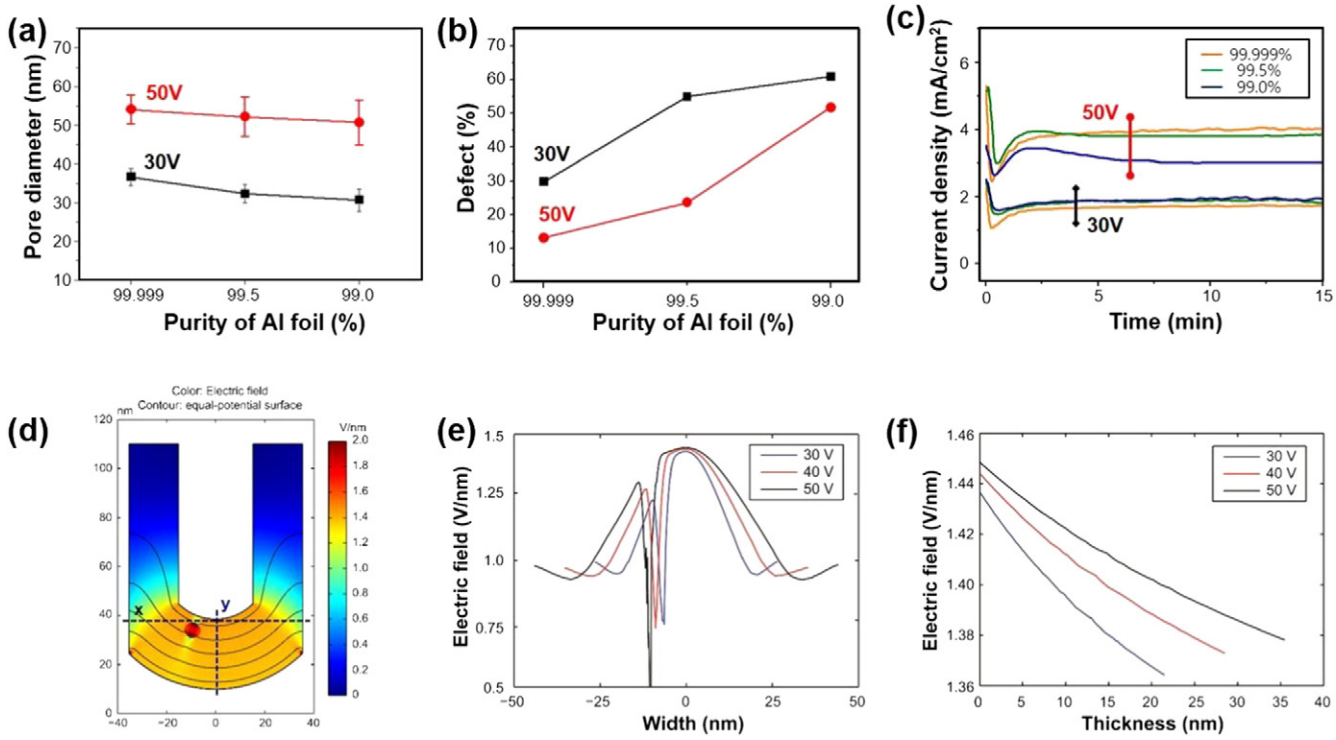

Fig. 3. Characteristic parameters of porous anodic alumina anodized using Al foils of different purity: (a) pore diameter, (b) defect (%), and (c) current density. (d) Electric-field distribution in the oxide with Si impurities. Electric-field distribution as a function of position along the (e) x-direction and (f) y-direction in (d), plotted for three different voltage.

50 V; Fig. 3a and b, respectively). Fig. 3c shows the current density as a function of time under a constant voltage (30 and 50 V) for the Al foils of different purity. Typically, the current density increases linearly with the applied voltage under the same experimental conditions; thus, the alumina films anodized at 50 V have a larger value. According to recent studies, the alloying elements can strongly affect the field-assisted dissolution of the oxide and the ionic resistivity of the oxide film; thus, the recorded steady-state current density is lower than that of pure Al [20]. The minimum of the current-density curve (at the beginning of the process) shows the growth of the compact and highly resistant oxide layer on Al, while the maximum (local increase after the minimum value) is a consequence of the rapid transformation of the compact layer to porous alumina, followed by a rearrangement of the pores on the surface [20]. Anodic alumina prepared from $Al_{99.5}$ and $Al_{99.0}$ at 50 V showed a shoulder at the maximum value (~2 min), indicating that impurities interrupt the rearrangement of pores during self-ordering. As a result, disordered-pore arrays were obtained in anodic films prepared from $Al_{99.5}$ and $Al_{99.0}$. The minimum current density required for $Al_{99.0}$ is lower because the impurities hinder the growth of the highly resistant oxide layer.

Furthermore, the defect-percentage trend can be explained in terms of current density. Significant differences in the current density did not clearly depend on the Al purity at 30 V; in contrast, drastic changes in the current density appeared at 50 V for $Al_{99.0}$. The difference in defect percentage between $Al_{99.999}$ and $Al_{99.0}$ at 30 V was ~31%; this increased to ~39% at 50 V. This behavior may be caused by the difference in the electric potentials between 30 and 50 V. We thus suggest that impurities can exert a greater effect at lower electric field, because the driving force for a straight-pore formation is lacking. Accordingly, the effect of the impurities on Al anodized at 30 V was stronger. We suggest that the defect percentage observed at 30 V is higher in all anodic alumina films (Fig. 3b), indicating that even a lower applied voltage may have a significant influence on the effect of the impurities. However, the largest difference between $Al_{99.5}$ and $Al_{99.0}$ at 50 V is caused by the low current density in $Al_{99.0}$; this indicates that the anodic alumina anodized at 50 V is less sensitive to impurities and its critical purity is in-between $Al_{99.5}$ and $Al_{99.0}$. Hence, impurities in the anodized alumina prepared from $Al_{99.5}$ exert a milder effect due to the high critical point at 50 V. Notably, the dependence of the electric-field distribution on the potential observed in the simulation supports the experimental results (Fig. 3d–f). In particular, we compared the electric-field distributions under various voltages along the x-direction (Fig. 3e) and y-direction (Fig. 3f). The different field distribution of the electric field is larger at 50 V than at 30 V, which is consistent with the experimental results. Considering the electric field requested for a straight-pore formation, these simulation data support that the straight-pore formation is limited at lower electric fields or lower voltages. Thus, our data, obtained from $Al_{99.5}$ and $Al_{99.0}$ at low applied voltage, confirm that pore formation is strongly affected by the impurities included in bulk Al. The impurities can affect the electric-field distribution, thereby inducing a branched-pore formation.

In summary, porous anodic alumina membranes fabricated from three types of Al foils with different purities (99.999%, 99.5%, and 99.0%) have been investigated using SEM imaging, EDX analysis, and simulations. The impurities in the Al foil have been shown to affect the process of pore formation; the percentage of defective pores increases proportionally with the impurity ratio. In addition, D_p values were smaller in lower-purity Al foils, and the standard deviation of D_p was larger. Moreover, impurities were confirmed to prevent pore formation; as a result, a reduced film thickness was obtained when using low-purity foils. The EDX analysis confirmed that the main components of the impurities are Si and Fe. The occluded impurities, which are located both on the surface and in the interior of the anodic alumina films, were observed to alter the original Al anodization flow pathway; moreover, impurities located inside the foil induced changes in the pore-formation process, resulting in the formation of more tilted pores. Finally, we showed that the purity of Al foils exerts a significant influence on the morphology of the alumina film, resulting in the formation of branched and tilted pores in the membrane. We believe that our impurity-driven pore formation approach provides important insights into the role of electric-field distribution in the fabrication of porous anodic alumina and a conceptual framework for the design and engineering the contact interface between biological cells and nanostructured materials.

Acknowledgments

This work was supported by Nano-Material Technology Development Program (2012M3A7B4034986) funded by the National Research Foundation and the Pioneer Research Center Program through the National Research Foundation of Korea funded by the Ministry of Science, ICT & Future Planning (2012-0009562). Additionally, it was supported by the Basic Science Research Program through the National Research Foundation of Korea funded by the Ministry of Science, ICT & Future Planning (2015R1A2A2A01005556).

Appendix A. Supplementary data

Experimental details, characteristic parameters, additional SEM images, and EDX data for the impurity-driven pore formation in porous anodic alumina. Supplementary data related to this article can be found at http://dx.doi.org/10.1016/j.scriptamat.2016.05.026.

References

[1] G.D. Sulka, A. Brzózka, L. Zaraska, M. Jaskuła, Electrochim. Acta 55 (2010) 4368–4376.
[2] W. Lee, R. Scholz, K. Nielsch, U. Gösele, Angew. Chem. Int. Ed. 44 (2005) 6050–6054.
[3] A. Johansson, T. Törndahl, L.M. Ottosson, M. Boman, J.-O. Carlsson, Mater. Sci. Eng. C 23 (2003) 823–826.
[4] J.E. Houser, K.R. Hebert, Nat. Mater. 8 (2009) 415–420.
[5] W. Lee, S.-J. Park, Chem. Rev. 114 (2014) 7487–7556.
[6] G.E. Thompson, Thin Solid Films 297 (1997) 192–201.
[7] S.J. Garcia-Vergera, P. Skeldon, G.E. Thompson, H. Habazaki, Electrochim. Acta 52 (2006) 681–687.
[8] J. Siejka, C. Ortega, J. Electrochem. Soc. 124 (1977) 883–891.
[9] J.P. Osullivan, G.C. Wood, Proc. R. Soc. London, Ser. A 317 (1970) 511–543.
[10] H. Masuda, K. Fukuda, Science 268 (1995) 1466–1468.
[11] S.M. Moon, S.I. Pyun, Electrochim. Acta 43 (1998) 3117–3126.
[12] S.J. Garcia-Vergara, P. Skeldon, G.E. Thompson, H. Habazaki, Corros. Sci. 49 (2007) 3772–3782.
[13] A.P. Li, F. Muller, A. Birner, K. Nielsch, U. Gosele, J. Appl. Phys. 84 (1998) 6023.
[14] F. Zhang, X. Liu, C. Pan, J. Zhu, Nanotechnology 18 (2007) 345302.
[15] C.-K. Chung, T.Y. Liu, W.T. Chang, Microsyst. Technol. 16 (2010) 1451–1456.
[16] A.L. Friedman, D. Brittain, L. Menon, J. Chem. Phys. 127 (2007) 154717.
[17] F. Zhou, A. Baron-Wiechec, S.J. Garcia-Vergara, M. Curioni, H. Habazaki, P. Skeldon, G.E. Thompson, Electrochim. Acta 59 (2012) 186–195.
[18] M.A. Kashi, A. Ramazani, J. Phys. D. Appl. Phys. 38 (2005) 2396–2399.
[19] C.C. Chen, J.H. Chen, C.G. Chao, Jpn. J. Appl. Phys. 44 (2005) 1529–1533.
[20] L. Zaraska, G.D. Sulka, J. Szeremeta, M. Jaskuła, Electrochim. Acta 55 (2010) 4377–4386.
[21] L.E. Fratila-Apachitei, F.D. Tichelaar, G.E. Thompson, H. Terryn, P. Skeldon, J. Duszczyk, L. Katgerman, Electrochim. Acta 49 (2004) 3169–3177.
[22] A.K. Mukhopadhyay, A.K. Sharma, Surf. Coat. Technol. 92 (1997) 212–220.
[23] D. Lo, R.A. Budimanz, J. Electrochem. Soc. 154 (2007) C60–C66.
[24] D. Li, L. Zhao, C. Jiang, J.G. Lu, Nano Lett. 10 (2010) 2766–2771.
[25] W. Lee, R. Ji, U. Gösele, K. Nielsch, Nat. Mater. 5 (2006) 741–747.
[26] C.-K. Chung, M.-W. Liao, C.-T. Lee, H.-C. Chang, Nanoscale Res. Lett. 6 (2011) 596.
[27] J.E. Houser, K.R. Hebert, J. Electrochem. Soc. 153 (2006) B566–B573.
[28] K. Shimizu, G.E. Thompson, G.C. Wood, Electrochim. Acta 27 (1982) 245–250.
[29] R.-L. Chiu, P.-H. Chang, C.-H. Tung, J. Electrochem. Soc. 142 (1995) 525–531.